Model Predictive Control Strategies in Switched Reluctance Motor Drives—An Overview

Jun Cai, *Senior Member, IEEE*, Xiaolan Dou, Adrian David Cheok, *Senior Member, IEEE*, Wen Ding, *Member, IEEE*, Ying Yan, *Member, IEEE*, and Xin Zhang, *Senior Member, IEEE*

***Abstract*—Model predictive control (MPC) is an advanced control technique with salient features, such as simplicity applied in multivariable systems, fast-transient response, inclusion of nonlinearities, and straightforward constraints in the control law, which is attracted in applying for high-performance control of motor drives. The electromagnetic characteristics of the switched reluctance motor (SRM) are of highly nonlinearity, which may result in lower control accuracy, slow stabilization time of control variables, unsatisfactory dynamic response, and torque ripples elimination performance. This article presents an overview of the current finite control set and continuous control set based MPC strategies in SRM drives. The model predictive current control, torque control, and flux control are analyzed from perspectives of modeling schemes, switching vectors optimization approaches, cost function selections, and the control performance. And finally, the current challenges and future development trends in applying the MPC technologies in SRM drives are also discussed.**

***Index Terms*—Continuous control set (CCS), finite control set (FCS), model predictive control (MPC), switched reluctance motor (SRM).**

I. Introduction

With the development and application of rare Earth or rare Earth free motor technology, switched reluctance motors (SRMs) are receiving increasing attentions. High speed, strong environmental adaptability, and high reliability are also important attractive features of SRM drives. However, due to their strong nonlinear characteristics, torque ripple, and vibration noise issues, the widespread application of SRMs has been hindered. The development and application of advanced control technologies in SRM drives are quite necessary for enhancing the overall operational performances [1].

In general, the traditional current chopping control (CCC), pulsewidth modulation control (PWM), and angle position control (APC) are widely used for driving the SRM. However, these methods only meet the basic rated operating conditions, and the torque ripple has not been effectively suppressed. To eliminate the torque ripple, the torque sharing function (TSF) based hysteresis current control [2], direct instantaneous torque hysteresis control [3], and direct torque control (DTC) [4] can be developed based on the traditional CCC and APC control. The essence of these control methods is to directly control torque or stabilize torque by shaping the phase currents. However, due to the highly nonlinear characteristic in SRM, the current tracking control has slow dynamic response, which makes it difficult to realize these optimized torque control strategies.

Model predictive control (MPC) is widely studied in recent years due to its salient features, such as the simplicity application in multivariable systems, fast transient response, inclusion of nonlinearities, and straightforward constraints in the control law [5], [6]. Based on the state combination of the controller and the physical characteristics of the controlled object, MPC can directly generate a power converter drive signal based on the predicted results, which is easy to reduce the switching frequency and has fast dynamic response. It has been successfully applied to permanent magnet synchronous motor (PMSM) and induction motor (IM) control [7], [8].

With the application of MPC technology in PMSM, this technology gradually introduced to SRMs, which also has great potential for application. In terms of current and torque control, a series of successful implementation cases of predictive control technology in SRM have been published in recent literature [9]. The review in [9] mainly focuses on the fundamental concepts of SRM drives, predictive control and the adopted classification, and a literature review of predictive current control strategies. Different from [9], in this article, the model predictive current control (MPCC), torque control, and flux control are fully analyzed from perspectives of modeling schemes, switching vectors optimization approaches, cost function selections, and the control performance. The main purpose of this review is to fully understand the operational mechanism of SRM control strategies based on MPC, so as to promote the application of high-performance SRM.

The rest of this article is organized as follows. In Section II, the basic concepts of SRM system are introduced. In Section III, the basic principle of MPC is described. In Section IV, the specific

Received 18 June 2024; accepted 21 August 2024. Date of publication 5 September 2024; date of current version 12 December 2024. This work was supported in part by the National Natural Science Foundation of China under Grant 52477055 and Grant 52077105, in part by the Natural Science Foundation of Jiangsu Province China under Grant BK20211285, and in part by the Excellent Research and Innovation Teams in Universities in Anhui Province under Grant 2023AH010021. Recommended for publication by Associate Editor D. Dujic. *(Corresponding author: Jun Cai.)*

Jun Cai is with C-MEIC, CICAEET, and the School of Automation, Nanjing University of Information Science and Technology, Nanjing 210044, China, and also with the Anhui Jianzhu University, Hefei 230009, China (e-mail: j.cai@nuist.edu.cn).

Xiaolan Dou, Adrian David Cheok, and Ying Yan are with C-MEIC, CICAEET, and the School of Automation, Nanjing University of Information Science and Technology, Nanjing 210044, China (e-mail: douxiaolan@nuist.edu.cn; adrian@imagineeringinstitute.org; ying.yan@nuist.edu.cn).

Wen Ding is with the Department of Electrical Engineering, Xi'an Jiaotong University, Xian 713599, China (e-mail: wending@xjtu.edu.cn).

Xin Zhang is with the College of Electrical Engineering, Zhejiang University, Hangzhou 310027, China (e-mail: zhangxin_ieee@zju.edu.cn).

Color versions of one or more figures in this article are available at https://doi.org/10.1109/TPEL.2024.3454819.

Digital Object Identifier 10.1109/TPEL.2024.3454819

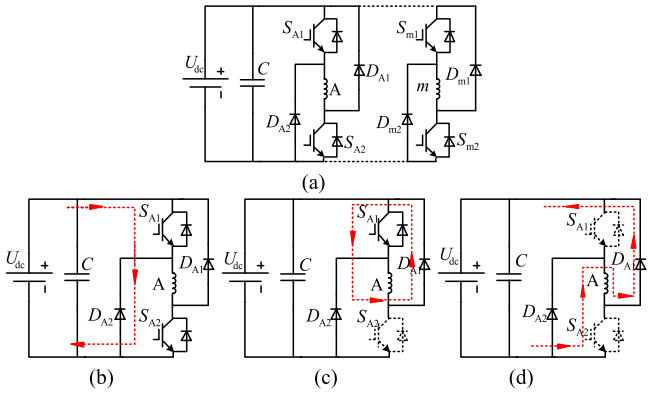

Fig. 1. Topology and the basic operational states for the AHB converter. (a) m-phase AHB converter. (b) +1 state. (c) 0 state. (d) −1 state.

work of MPC-based SRM control strategies are analyzed in detail. The typical challenges in MPC realization and its solutions are discussed in Section V. The future trends and challenges of developing the MPC technology in SRM drive systems are discussed in Section VI. Finally, Section VII concludes this article.

II. Fundamentals of SRM Drives

Generally, the asymmetric half-bridge power converter (AHB) has the characteristics of phase independence, flexible control, and easy expansion of the number of motor phases, which is the most commonly used power converter for SRM drives [1]. The basic topology and the basic operational states of the AHB converter is shown in Fig. 1.

As shown in Fig. 1, each phase-leg of the AHB converter can be driven independently without bridge arm straight-through problem, which makes the SRM system more reliable. Basically, the AHB converter consists of three operational states: the magnetization state (+1 state), the free-wheeling state (0 state), and the demagnetization state (−1 sate). The three operational states are shown in Fig. 1. In +1 state, the two switches of the bridge leg are turned-ON simultaneously, and the voltage applied to the phase winding is $+U_{\rm dc}$. In 0 state, only one of the power switches is turned-ON to let the phase current freewheeling in zero-voltage state. In −1 state, both of the two power switches are turned-OFF and the voltage applied in the phase winding is $-U_{\rm dc}$, which can ensure fast demagnetization. The phase voltage equation of the three operational states can be represented by

$$SU_{dc} = Ri + L(i,\theta)\frac{di}{dt} + i\omega\frac{\partial L(i,\theta)}{\partial\theta} \tag{1}$$

where $U_{\rm dc}$ and i are the bus voltage and the phase current, respectively. R is the winding resistance, and L is the phase inductance, which is a nonlinear function of the phase current and position angle θ. $S = 1$, 0, and −1 denotes the three operational states, respectively.

In addition, the electromagnetic torque can be obtained by taking the angle partial differentiation with respect to the magnetic common energy

$$T_e = \partial W'/\partial\theta \tag{2}$$

where T_e is the electromagnetic torque. W' is the magnetic common energy, which can be calculated by

$$W'(i,\theta) = \int_0^i L(i,\theta)idi. \tag{3}$$

III. Fundamentals of Model Predictive Control

A. The Basic Principle of the Generalized MPC

The basic idea of MPC is to solve the following optimal control problems at each time step in the finite time domain. The most important feature is that the objective function can be optimized and the constraints of the system can be integrated and processed in a systematic way, and the online optimization can be achieved through rolling optimization.

A generic nonlinear state-space system can be expressed as

$$\begin{aligned} x_{k+1} &= f(x_k, u_k) + \omega_{p,k} \\ y_k &= g(x_k) + \omega_{m,k} \end{aligned} \tag{4}$$

where x_k is the state vector, u_k is the control vector, y_k is the measurement vector, $w_{p,k}$ is the unknown process noise, and $w_{m,k}$ is the unknown measurement noise at time instant $t_k = kT_s$, where T_s is the sampling period. The functions f and g describe the plant dynamics and measurement process, respectively.

Generally, the MPC is defined by the constrained finite time optimal control problem with a quadratic cost function [10]

$$\underset{\substack{u_0,\ldots,u_{N-1}\\ x_1,\ldots,x_N}}{\arg\min}\ e'_{x,N}P_c e_{x,N} + \sum_{j=0}^{N-1} e'_{x,j}Q_c e_{x,j} + \sum_{j=0}^{N-1} e'_{u,j}R_c e_{u,j} \tag{5}$$

where

$$\begin{cases} e_{x,j} = x_j - \bar{x}_j \\ e_{u,j} = u_j - \bar{u}_j \\ x_{j+1} = f(x_j, u_j) \end{cases} \tag{6}$$

where j is the sampling instant $t = (k + j)T_s$, $j = 0$ denotes the sampling instant when the controller is operated, and $j > 0$ are the predicted sampling instances. Q_c and R are positive definite symmetric weighting matrices, which can define the cost function and penalize state errors, respectively. P_c is the terminal cost, which links the properties of the finite time MPC with infinite time linear quadratic regulator (LQR). $e_{x,j}$ and $e_{u,j}$ are the state and tracking error, respectively; and $\bar{x}_j$ and $\bar{u}_j$ denote the desired steady-state reference. The problem (5) can be solved from the control sequences $u_0, \ldots, u_{N-1}$ and the state sequences $x_1, \ldots, x_N$. The MPC applies the first optimal control values u^*_0 to the plant, then the (5) is solved with receded horizon at the next instant.

The basic idea of MPC includes the following three steps, and its basic control block diagram is shown in Fig. 2. The $y(k + j)$ is the output variable with future behavior, which is a function of the input $u(k)$ and the desired reference Γ^*. The specific steps are as follows.

1) Use the prediction model to predict the future dynamics of the system over a limited period of time.
2) Use a cost function to represent the expected system behavior and optimize the cost function for solution.

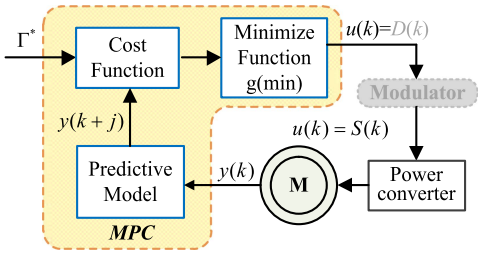

Fig. 2. Basic control block diagram of the MPC.

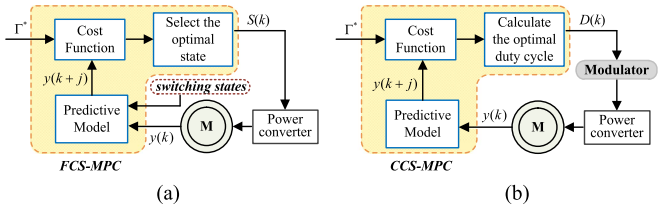

Fig. 3. Basic control block diagram of the FCS and CCS MPC. (a) FCS–MPC (b) CCS–MPC.

3) Apply the first element of the optimization solution to the system.

B. Development and Classification of MPC

The MPC was originally studied and applied in process control [11]. In recent years, MPC is widely applied in power electronics and motor drives [5], [6], [12], [13]. Normally, two typical approaches, such as the finite control set (FCS–MPC) and continuous control set MPC (CCS–MPC) are the most attracted methods in motor drive applications.

In general, the FCS–MPC requires more complicated real-time calculations to solve optimization problems online, while the procedure of optimization in CCS–MPC is implemented offline. FCS–MPC implements a cost function with discrete states. As shown in Fig. 3(a), possible switching states are applied as inputs to the power converters and several possible outcomes can be obtained, then the corresponding switching state with the minimum cost function can be selected for driving. The FCS–MPC can ensure faster dynamic responses. However, the calculation burden is high due to the multivector traversal and the switching frequency is variable without applying a modulator [14].

Unlike the FCS–MPC, the CCS–MPC implements a cost function with continuous states. As shown in Fig. 3(b), the predicted value and the desired reference are fed to the cost function, and the control signal can be calculated based on the cost function minimization strategy. The control signal in the form of duty cycle can then feed in a modulator to generate a fixed switching frequency.

IV. Model Predictive Control Strategies and Applications in SRM

In recent years, several studies have been attempted in applying the MPC in SRM drives, which can be mainly classified into three types, such as the MPCC, model predictive torque control (MPTC), and model predictive flux control (MPFC). The detailed overview of these control algorithms are as follows.

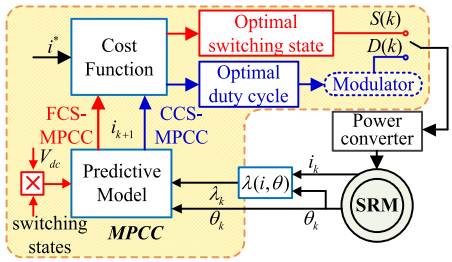

Fig. 4. Block diagram of MPCC of SRM.

A. MPCC Control in SRM

Traditionally, due to the highly nonlinear behaviors of the phase inductances and flux linkage, the electromagnetic saturation would affect the phase current irregularly, which makes it difficult to ensure the current tracking performance. Correspondingly, the poor current tracking capability in traditional CCC control may result in increased torque ripple and acoustic noise. Aiming at this problem, the MPCC control strategies are studied in SRM.

1) Basic Principle of the MPCC: Based on the phase voltage (1), the predicted value of the current can be obtained by making a first-order difference of *di/dt*

$$i_{k+1} = i_k + \frac{T_s}{L_k}[v_k - Ri_k - i_k\omega(\partial L_k/\partial\theta_k)] \tag{7}$$

where θ_k is the position angle at kth moment, and i_k and i_{k+1} are the phase current at k and $k+1$th moment, respectively. L_k and v_k are phase inductance and phase voltage at kth moment, respectively. T_s is sampling period.

As shown in Fig. 4, the algorithm of a general MPCC starts with the measurement of phase current $i(k)$ and rotor position $\theta(k)$. Then, the predictive model estimates the phase current in the next sampling period, which is based on the previous states and the machine parameters. The predicted state in this case is the current $x(k+1) = i(k+1)$. The cost function is optional as CCS–MPC can calculate the duty cycle directly. The output control signal $u(k)$ can be generated either by a modulator or selecting the switching pattern directly [15].

2) MPCC Applications in SRM: An accurate model in MPCC guarantees a proper tracking response for both transient and steady-state operation. How to obtain the current sampling value efficiently is a subject worth studying. In [16], the author presents a fixed-switching-frequency MPCC using time-multiplexed current sensor for SRM drives. Satisfied current sampling can be achieved with a single current senor and minor tracking errors exist as compared with a traditional hysteresis current controller.

Due to the highly nonlinearity in SRM, the inductance modeling is also a challenge, which is also an important fact to affect the current predict accuracy. If the saturation is neglected, the inductance is simple function of the rotor position [17], [18], [19]. However, if the saturation is taken into consideration, the inductance is a nonlinear function of both the phase current and rotor position [20], [21]. In [22], an inductance surface estimation and learning for utilization with a stochastic MPC scheme for the current control of SRMs is introduced. As shown in Fig. 5, a learning mechanism is developed to dynamically adapt

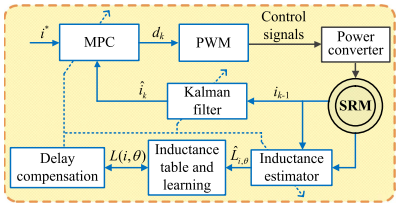

Fig. 5. Control block diagram of [22].

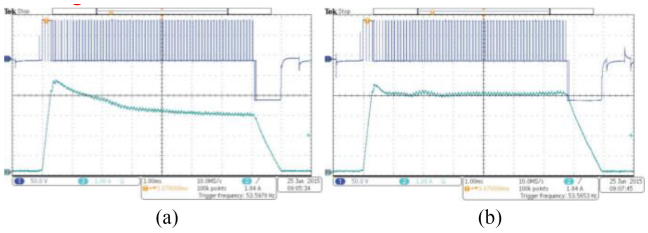

Fig. 6. Experimental result in [22]. (a) With on inductance learning activated. (b) Inductance learning activated.

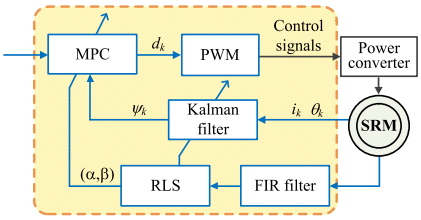

Fig. 7. Control block diagram of [23].

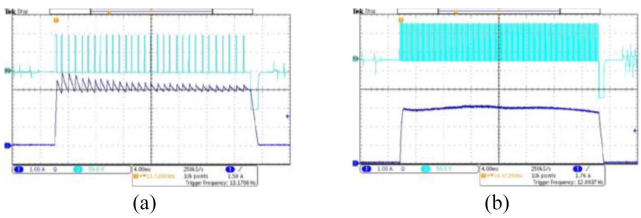

Fig. 8. Experimental result in [23]. (a) Delta-modulation. (b) LQR.

to the inductance profile of the machine and update the MPC and Kalman filter parameters. This mechanism is combined with the CCS–MPC, which can benefit from a fixed switching frequency and offer low current ripples by calculating the optimal duty cycles using the SRM model.

Fig. 6 shows the experimental results before and after using the learning mechanism at a speed of 400 rpm and a reference current of 4 A, which illustrate the effectiveness of the proposed method in learning the profile and reducing the tracking error of MPC.

Similarly, an unconstrained MPC known as a finite horizon LQR for current control of an SRM is investigated in [23]. As shown in Fig. 7, the Kalman filtering is used for state estimation while an adaptive controller is used to dynamically tune and update both MPC and Kalman models.

This scheme uses an adaptive calibrator to compensate for the inductance and resistance mismatch between the model and the physical system. The performance of the system at 100 rpm is investigated. Fig. 8(a) shows the behavior of the

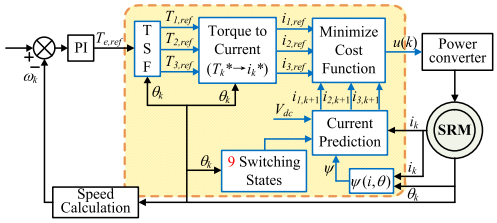

Fig. 9. Control block diagram of FCS–MPCC in [24].

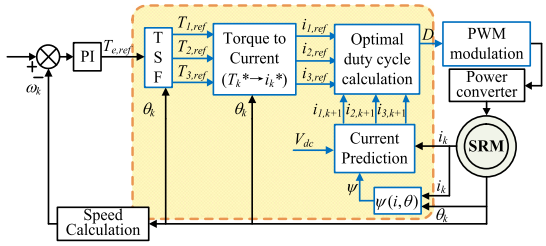

Fig. 10. Control block diagram of CCS–MPCC in [24].

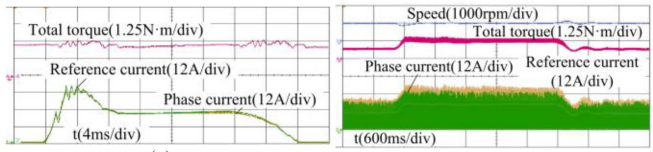

Fig. 11. Experimental result of CCS–MPCC in [24]: (a) steady-state and (b) dynamic response.

delta-modulation and using LQR, the large ripples induced by delta-modulation is reduced as shown in Fig. 8(b).

To improve the computation efficiency of the FCS–MPCC scheme, the switching states need to be optimized according to the commutation logics of the SRM. As shown in Fig. 9, a TSF-based FCS–MPCC with optimized switching states is proposed in [24]. As compared with traditional FCS–MPCC, the number of the available switching states is reduced from 27 to 9.

In [24], a TSF-based CCS–MPCC is also discussed. As shown in Fig. 10, the optimal solution was carried out according to the selected objective function and the optimal voltage duty ratio was directly calculated. As the switching frequency can be controlled in this scheme, the current tracking performance would be highly improved and thus the torque ripple is much lower. The experimental results are shown in Fig. 11, indicating the effectiveness of the algorithm.

B. MPTC Control in SRM

1) Torque Predictive Model: A torque modeling method in [25] and [26] is employed and the torque can be expressed as

$$\begin{cases} i_{k+1} = i_k + \frac{T_s}{\partial\psi_k/\partial i_k}\left[v_k - Ri_k - \frac{\partial\psi_k}{\partial\theta_k}\omega\right] \\ T_{k+1} = \left[\frac{L_{dsat}-L_q}{2}i_{k+1}^2 + Ai_{k+1} - \frac{B}{A}\left(1-e^{-Bi_{k+1}}\right)\right] \\ \qquad f'(\theta_{k+1}) \end{cases} \tag{8}$$

where T_k is phase torque at kth moment, T_{k+1}, i_{k+1}, and θ_{k+1} are phase torque, phase current, and the position angle at k+1th

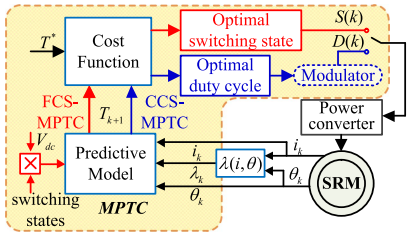

Fig. 12. Block diagram of MPTC of SRM.

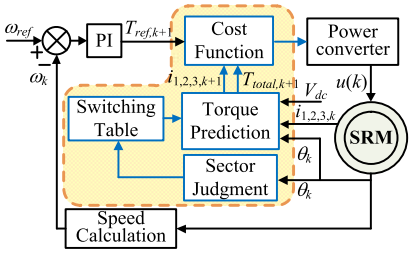

Fig. 13. Control block diagram of FCS–MPTC in [29] and [30].

moment, respectively, and A, B, and ψ_k can be denoted as

$$\begin{cases} A = \psi_m - L_{dsat} i_m \\ B = (L_d - L_{dsat})/(\psi_m - L_{dsat} i_m) \\ \psi_k = L_q i_k + \left[L_{dsat} i_k + A(1 - e^{-Bi_k}) - L_q i_k \right] f(\theta_k) \end{cases} \tag{9}$$

where L_q is the inductance at the unaligned position, L_d is the inductance when phase current i is less than saturated phase current i_s, and L_{dsat} is the inductance value corresponding to the saturation current i_m at the aligned position. i_m is the maximum current in stator windings and ψ_m is the flux linkage at $i = i_m$. $f(\theta)$ is a nonlinear function which deduces the flux-linkage characteristics corresponding to the rotor positions between the aligned and unaligned rotor position [27] as follows:

$$f(\theta) = 2N_r^3\theta^3/\pi^3 - 3N_r^2\theta^2/\pi^2 + 1 \tag{10}$$

where N_r is the number of rotor pole.

As shown in Fig. 12, the MPTC algorithm uses the measured phase current $i(k)$ and rotor position $\theta(k)$ to feed the predictive model and estimate the torque output $T(k+1)$. The predicted torque values are then used in a cost function to decide which of the switching state provides the minimum error with respect to the torque reference [27], [28].

2) MPTC Applications in SRM: In [28], an FCS–MPTC is applied for DTC. In this method, the phase currents $i(k+1)$ is also predicted and controlled as a secondary objective. This effort can ensure reduced copper losses.

In [29] and [30], an improved FCS–MPTC for SRM drives is proposed in which a new switching table is constructed by using the sector partition technique to reduce the computational burden, as shown in Fig. 13. It removes the flux linkage calculation compared to conventional FCS–MPTC. The electric cycle of SRM is divided into six sectors based on the negative torque contribution of each phase and the commutation region of the motor is redefined. Voltage vectors of each sector are optimized in terms of phase torque characteristics and the number of voltage vectors is reduced to 2 or 3 at each control period. The proposed FCS–MPTC method effectively reduces the torque ripple and the generation of negative torque, which improves torque–ampere ratio and the efficiency of the system.

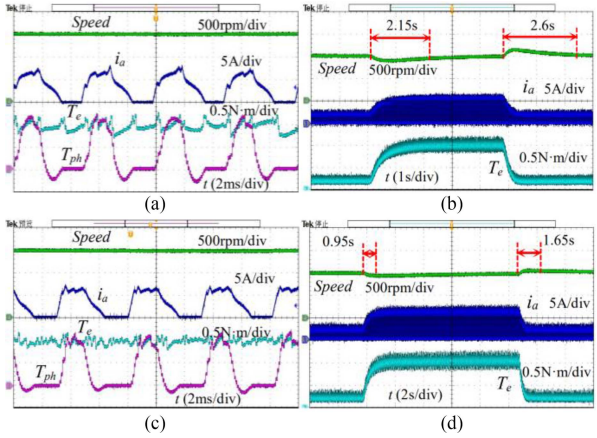

Fig. 14. Experimental result in [29]: (a) steady-state-DTC, (b) dynamic response-DTC, (c) steady-state-MPTC, and (d) dynamic response-MPTC.

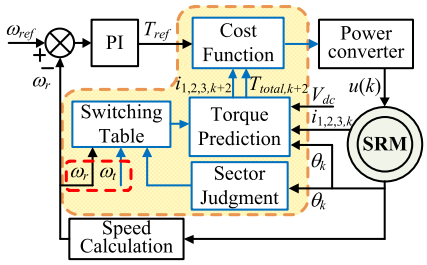

Fig. 15. Control block diagram of FCS–MPTC in [31].

Fig. 14 shows the steady-state and dynamic experimental results of MPTC in [29], which indicate that compared with DTC, the proposed MPTC has a higher torque per ampere ratio and less copper loss for the same output power, and can greatly decrease the torque ripple and enhance the system efficiency of the SRM. When load disturbance occurs, it can perform better stability and tracking feature when the load changes.

Heavy computation burden and degraded high-speed torque control performance are the main issues for the conventional look-up-table (LUT)-based MPTC method. In [31], to ease these issues, an improved switching table is proposed to reduce the computational time by 25% compared to the conventional method and enhance the high-speed torque control performance, as shown in Fig. 15. To further reduce the storage space of the LUT-based MPTC method, the linear-model-based MPTC method is proposed based on the developed flux-linkage and torque transformation. This proposed method requires only 228 storage units compared to 1530 storage units consumption of the LUT-based methods.

The experimental results in Fig. 16(a) indicate that the low-frequency commutation torque ripple is significantly reduced, and the high-frequency torque ripple results from the CCC by the MPTC.

It is notorious that only cost functions and direct calculations are implemented in MPTC for SRM to obtain the actuating variable of the control loop. Use the predictive model to define the switching pattern in form of a reference voltage. For instance,

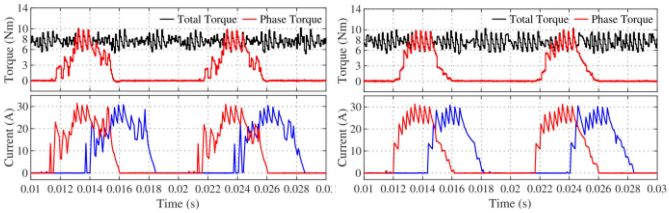

Fig. 16. Experimental result in [31]. (a) LUT-based MPTC in [28]. (b) Linear-model-based MPTC in [31].

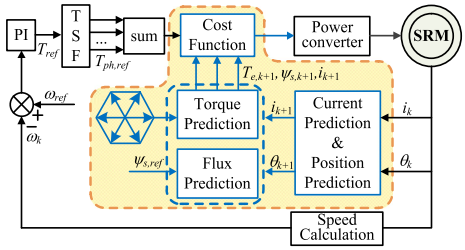

Fig. 17. Control block diagram of FCS–MPDTC in [32].

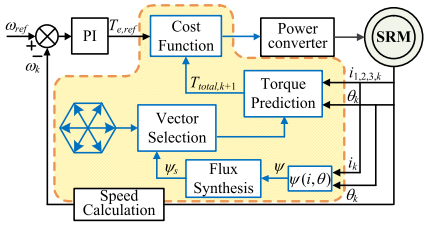

Fig. 18. Control block diagram of FCS–MPTC in [25].

according to the combination of FCS–MPC and DTC methods, some DTC-based FCS–MPC strategies are proposed.

In [32], an FCS–MPDTC method is proposed. In this article, the conventional DTC with double hysteresis control is replaced by the proposed MPDTC to reduce torque ripple and improve the dynamic performance of segmented SRM. As shown in Fig. 17, considering torque ripple reduction, flux tracking performance, and copper losses reduction, the cost function with phase torque, the amplitude of flux linkage, and phase current is established to select optimal voltage vector. In addition, the TSF is employed to distribute total torque to phase torque for further torque ripple reduction. The optimal voltage vector is obtained through the following cost function:

$$\min J(u_k) = q_1(T_{e,k+1} - T_{e,\text{ref}})^2 + q_2 \sum i_{k+1}^2 + q_3(\psi_{s,k+1} - \psi_{s,\text{ref}})^2 + q_4(s_{k+1} - s_k) \quad (11)$$

where q_1, q_2, q_3, and q_4 are weight factors that are ensured corresponding to control objects [33], [34]. The $\psi_{s,\text{ref}}$, $T_{e,\text{ref}}$ and $\psi_{s,k+1}$, $T_{e,k+1}$ are amplitude of reference flux and torque and predicted flux and torque, respectively, and s is the switching times.

An improved DTC-based FCS–MPTC algorithm has been proposed in [25]. As shown in Fig. 18, by using the method of sector division and voltage vector selection of DTC, the sector is judged by flux linkage signal, and the voltage vector is selected as the input of predictive control.

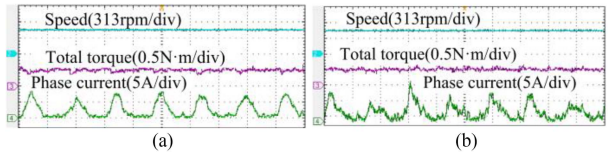

Fig. 19. Experimental result in [25]. (a) Traditional MPTC. (b) MPTC proposed in [25].

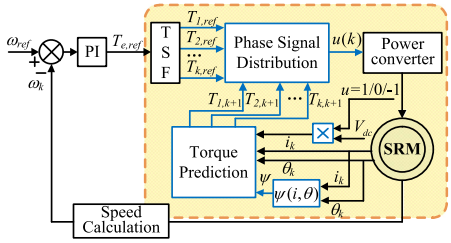

Fig. 20. Control block diagram of model prediction based DITC in [40].

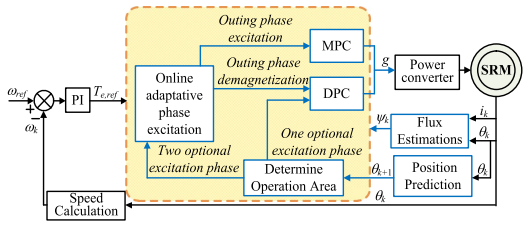

Fig. 21. Control block diagram of [41].

According to the experimental results shown in Fig. 19, it can be concluded that compared to traditional MPTC, DTC-based FCS–MPTC in [25] has a shorter control cycle, fixed switching frequency, and lower torque ripple.

In [35], an online direct instantaneous torque control (DITC) technique is proposed. In this method, the torque is estimated as a function of flux linkage and phase current. In addition, a digital torque hysteresis controller is implemented with high-bandwidth drive performance. Thus, the method can operate without torque functions. Using DITC, the torque ripple can be largely reduced [36], [37], [38], [39].

Due to the highly nonlinearity in SRMs, it is too difficult to consider the limitations, such as inductance, control period, and so on. As the future flux by each of various gate signals can be predicted, the future current and torque can then be predicted easily. Thus, the most suitable gate signal can be chosen from the predicted behavior. In [40], the method of model prediction based DITC is proposed, which has simpler logic and better control effect. This method could reduce torque ripple in wide speed range and provided good efficiency drive. Fig. 20 shows the block diagram of the method.

In [41], a four-quadrant operation strategy is proposed to enhance the performance of the SRM in the high-dynamic speed adjustment applications. As shown in Fig. 21, the core of the proposed method is a PWM-based predictive control method with the online adaptive phase excitation which is composed of the MPC and deadbeat predictive control (DPC). The MPC is applied in the commutation region and the DPC is used to calculate the control signal for the single-phase excitation and the four-quadrant operation of the SRM for the high-dynamic

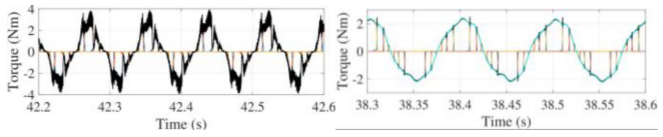

Fig. 22. Experimental result in [41]. (a) CCC. (b) Method in [41].

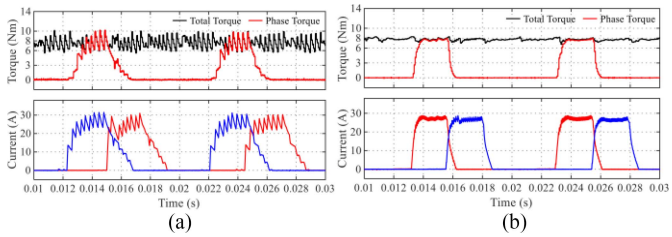

Fig. 23. Experimental result in [42]. (a) FCS–MPTC in [31]. (b) CCS–MPTC in [42].

speed adjustment application is realized. This method employs nine states of duty cycle as a finite set to reduce the computational burden and save hardware resources. Fig. 22 shows that compared to CCC, the output torque can track the reference torque well. During the commutation, torque ripple is reduced and the outgoing phase is never turned OFF too late.

In [42], a low-ripple CCS–MPTC method is proposed. The inherent high nonlinearity of the SRMs makes it difficult to solve the optimization problem in the CCS–MPTC. To address highly nonlinearity issues, an equivalent linear SRM (LSRM) model is adopted, and the cost function is modified. With the torque boundary values provided by executing the voltage vectors of an improved switching table, the optimization process for CCS–MPTC is simplified and solvable. The Lagrange multiplier method is also employed for analytically solving the optimization problem analytically and generating the optimum torque reference values for the active phases. Based on the estimated torque variation rates, the duty cycles for each phase can be calculated. Fig. 23 shows the excellent torque control performance of the CCS–MPTC method in [42].

C. MPFC Control in SRM

Different from those of IM or PMSM, the torque ripple in SRM is mainly due to the highly nonlinear torque and magnetization characteristics. To be more specific, the instantaneous torque in the SRM mainly depends on the partial derivative of stator flux linkage with respect to the angle, which means there is a one-step delay between the torque and the flux. Thus, if the flux linkage can be controlled in advance, the torque ripple will be significantly reduced.

In [43] and [44], to solve the problem of large torque ripple in a SRM, an MPFC–DTC control scheme is proposed. The control block diagram is shown in Fig. 24. The predicted flux linkage is calculated from the discrete time model of the SRM. To reduce the computation burden and increase the dynamic response, a torque hysteresis controller is embedded to select the candidate voltage vectors for the cost function. Finally, based on flux linkage minimization, the optimal voltage vector is selected. This method shows better steady-state and dynamic-state performances compared to traditional DTC. As shown in Fig. 25, the

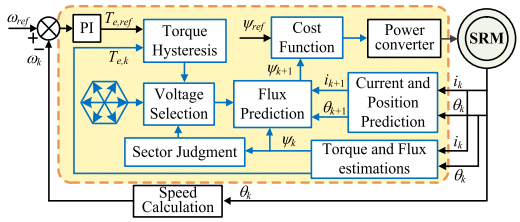

Fig. 24. Control block diagram of MPFC–DTC in [43] and [44].

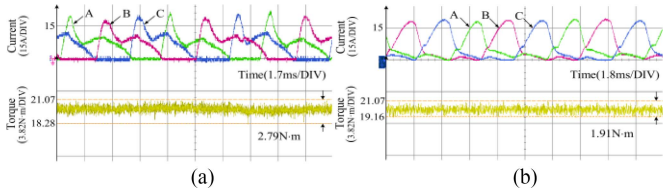

Fig. 25. Experimental result in [43]. (a) DITC. (b) MPFC in [43].

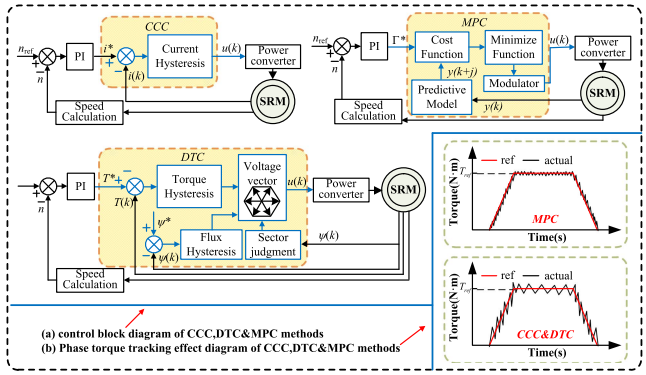

Fig. 26. Comparison of control block diagram of three methods.

MPFC–DTC can partly overcome the torque ripple compared with the DITC method.

D. Comparison of the MPC With Traditional CCC and DTC

Generally, the CCC is the most widely used control scheme for SRM. The CCC control performance is highly affected by the selected hysteresis band, rotational speed, the current sampling period, and control interrupt period in the controller. The current tracking control frequency is also varied instantaneously, which is unsuitable for eliminating the torque ripple. The traditional DTC introduces hysteresis control into torque regulation, which also has varied switching frequency and degradation control performance at high speed [45]. The comparison of control block diagram of CCC, DTC, and MPC is shown in Fig. 26. As can be seen in this figure, the MPC can achieve fixed switching frequency by modulator, which can ensure better torque ripple suppression effect.

E. Summary

Based on the various optimized MPC strategies mentioned above, for FCS–MPC, fewer candidate switch state combinations can reduce the complexity of the control algorithm, reduce computational pressure, and enhance the torque ripple suppression ability of the algorithm control effect. However, it is difficult to achieve a fixed control frequency. CCS–MPC breaks free

TABLE I
COMPARISON OF THE DIFFERENT MPC METHODS

features \ methods	MPCC in [22]	MPTC in [25]	MPTC in [29]	MPTC in [31]	MPTC in [33]	MPFC in [43]
Complexity	Complex	Medium	Medium	Complex	Medium	Medium
Fixed switching frequency	Yes	Yes	No	No	No	No
Number of switching states	--	2	2/3	6	9	4
Torque ripple	Medium	Medium	Low	Medium	Low	Low

-- indicates that the variable does not exist.

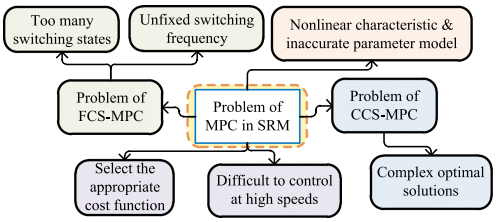

Fig. 27. Problems of MPC in SRM.

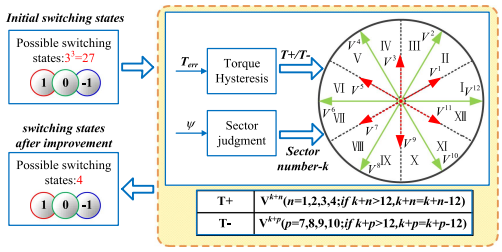

Fig. 28. Optimization scheme diagram of [43].

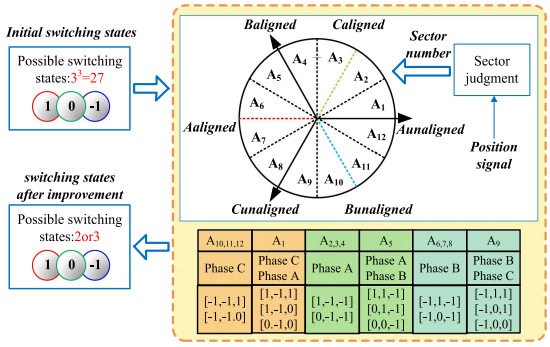

Fig. 29. Optimization scheme diagram of [29] and [30].

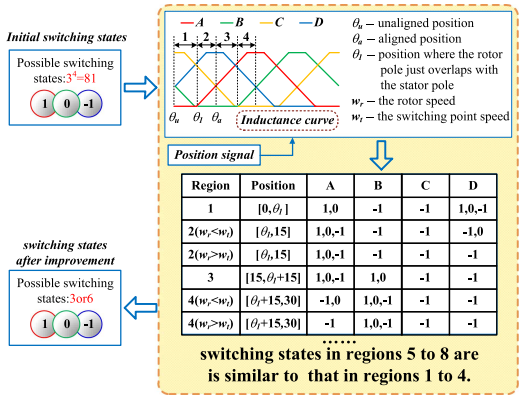

Fig. 30. Optimization scheme diagram of [31].

from the constraints of candidate switch state combinations and achieves a fixed control frequency, but the algorithm complexity increases accordingly. Table I summarizes and compares the characteristics of some representative MPC strategies.

V. MAIN ISSUES AND SOLUTIONS OF MPC IN SRM

Fig. 27 shows the main issues of the MPC in SRM drives. As illustrated in this figure, the MPC algorithm always suffers from the nonaccurate electromagnetic parameter model and difficulty of selecting cost functions. The main drawbacks of the FCS–MPC are the unfixed switching frequency and high computational burden. But the CCS–MPC is also affected by the complex optimal solutions. The systematical analyses of the solutions of these issues are as follows.

A. Main Issues and Solutions for FCS–MPC

To improve the overall performance of the FCS–MPC, it is necessary to optimize the switching states and ensure fixed switching frequency.

1) Optimize the Switching States: Based on the DTC strategy in SRM that the selection of control vectors varies in different flux linkage angle intervals, an MPC controller is used to replace the traditional DTC's magnetic flux hysteresis control or torque hysteresis control and the candidate control vectors are used as the MPC candidate switch state set. This type of strategy can improve the dynamic response speed, suppress torque ripple compared to traditional DTC, and reduce the computational burden caused by a large number of candidate switch states in traditional MPC. The specific process is shown in Fig. 28, by using the method of sector division and voltage vector selection of DTC, the increasing and decreasing torque vectors of each sector are set in advance, and these vectors are used as input variables of torque control prediction by torque hysteresis signal, which greatly reduces the number of switching states [43]. Similar methods are proposed in [25] and [44].

On the premise of ensuring the efficiency of the motor, the conduction states of each phase of the motor can be limited according to the different position angles, and the restricted conduction states of each phase can be combined to reduce the number of switch state combinations [29], [30], as shown in Fig. 29. According to the characteristics of SRM phase separation conduction, two-phase can be conducted simultaneously at most, then different position angle intervals can be divided. In different position sectors, some restricted switch state combinations are inefficient or even ineffective, so filtering can be performed to further reduce the number of switch state combinations. Similar methods are discussed in [33], [46], and [47].

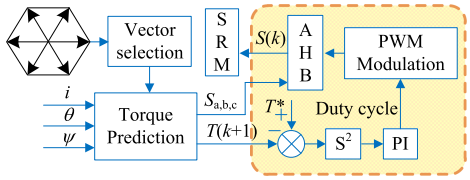

Fig. 31. Optimization scheme diagram of [25].

As shown in Fig. 30, an improved switching table with only six switching states is developed in [31] for a four phase 8/6 structure SRM based on the inductance characteristics partition logics. The adoption of this improved switching table not only reduces the computational burden by 25% but also improves the torque control performance and system efficiency at high-speed region.

2) Fix Switching Frequency: In [25], an FCS–MPTC method assisted with duty ratio modulation is proposed. As shown in Fig. 31, a PI regulator is utilized to generate a duty ratio for PWM modulation. The modulated signals are combined with the FCS–MPTC estimated switching signals to drive the SRM. As compared with traditional DTC and FCS–MPTC, the switching frequency here is fixed through PWM modulation, and thus the torque ripple and copper losses can be lowered better.

B. Main Issues and Solutions for CCS–MPC

To improve the overall performance of the CCS–MPC, it is necessary to optimize the process of obtaining the optimal solution and enhance ability to control high-speed SRM.

1) Optimize the Process of Obtaining the Optimal Solution: In [42], to address this issue, an equivalent LSRM model is adopted, and the cost function is also properly modified. Then, with the torque boundary values provided by executing the voltage vectors of an improved switching table, the optimization problem in the CCS–MPTC method becomes simple and analytically solvable, which shorten the algorithm execution time and reduces the computational pressure of optimal control. In [23], the authors proposed an MPC with Kalman filter and automatic calibration of inductor profile. Additionally, to cope with model variations, two adaptive gains were dynamically calculated to compensate for the inductance and resistance mismatch between the model and the physical system. The overall control structure can be considered as a stochastic CCS–MPC with adaptive model calibration, which makes the calculation of optimal control signal more accurate.

2) Improve the High-Speed Control Capabilities: The traditional method for controlling high-speed and high-power SRM is to design an SRM with low-phase inductance to provide sufficient current rise in a short period of time. However, this design generates significant current fluctuations at low speeds due to excessively high switching frequencies, leading to SRM loss of control. The method in [22] not only improves the accuracy of inductance, but also introduces a delay compensation technique to handle measurement delays in MPC of an SRM to expand speed range of SRM operation.

C. Nonlinear Characteristic and Parameter Model of SRM

The nonlinear characteristics of SRM make it difficult to be controlled. In addition, when MPC is used to control SRM, various parameters of the motor, such as torque, flux, inductance, etc., are required and it is difficult to get the accurate parametric model. It is necessary to find a way to obtain accurate parameters and the following are some of the methods available.

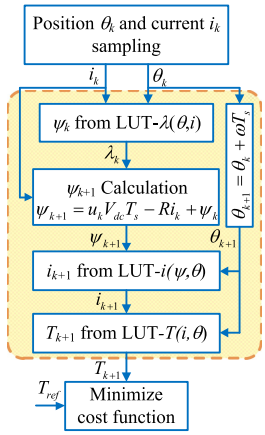

Fig. 32. Flow chart for LUT-based MPTC.

1) Magnetic Characteristic Date Acquisition: The premise of establishing parameter model is to obtain accurate parameter data. The commonly used modeling methods are mainly divided into finite-element analysis (FEA) and multipoint data fitting. The method of actual measurement data is divided into direct and indirect types. In the direct category, the parameter data can be measured directly through the sensor without satisfactory precision. However, the indirect method of measuring the phase voltage and current and then calculating the required flux and torque data provides better accuracy [48]. The flux linkage ($\psi_{\rm ph}$) can be calculated indirectly from the online phase voltage and current measurements using

$$\psi_{\rm ph}(t) = \int_0^t (V_{\rm ph}(t) - R_s i_{\rm ph}(t))dt + \psi_{\rm ph}(0) \qquad (12)$$

where $V_{\rm ph}(t)$ and $i_{\rm ph}(t)$ are the measured phase voltage and current, respectively. The initial flux linkage $\psi_{\rm ph}(0) = 0$, given $i_{\rm ph}(0) = 0$. This simple direct flux calculation method has been widely used in SRM drivers [49]. However, the problem that the initial magnetic flux is not zero due to the residual magnetic flux [50] remains to be solved.

In order to reduce the difficulty of data acquisition and increase the accuracy of data, scholars have put forward a lot of improvement methods. A torque balance measurement method according to the symmetric structure of SRM and some torque balance positions is proposed [51], which greatly reduced the workload and cost of obtaining flux value. Some scholars have proposed a constant current injection method that does not require a fixed rotor position. It keeps the phase current constant while running at a constant speed to obtain complete machine characteristics including characteristics of back electromotive force, flux, and torque [52].

2) Look-Up-Table Method: The traditional method to obtain parameters is to LUTs of various parameters which include the two-dimensional (2-D) flux-linkage ψ (θ, i), current $i(\psi, \theta)$, and torque $T(\theta, i)$. The specific process of MPTC is shown in Fig. 32 as an example. LUTs not only preserve the accuracy of the SRM model but also possess a low computational burden. However, the LUT method occupies too much memory space

TABLE II
REPRESENTATIVE MODELING METHODS

Ref.	Methods		Complexity	Precision
[53], [54], [55]	Mathematic modeling	Exponential function	Low	Medium
[56]		Fourth-degree polynomial	Low	Medium
[57]-[59]		Fourier series	Medium	Medium
[18]		Hermite interpolation	Low	Medium
[61]	Neural network modeling	ANFIS	High	Medium
		BPNN	High	Medium
		RBF	Medium	High
[60]		BSNN	High	High
[22]	Inductance learning mechanism		High	High
[62]	Unsaturated inductance reconstruction		Medium	Medium

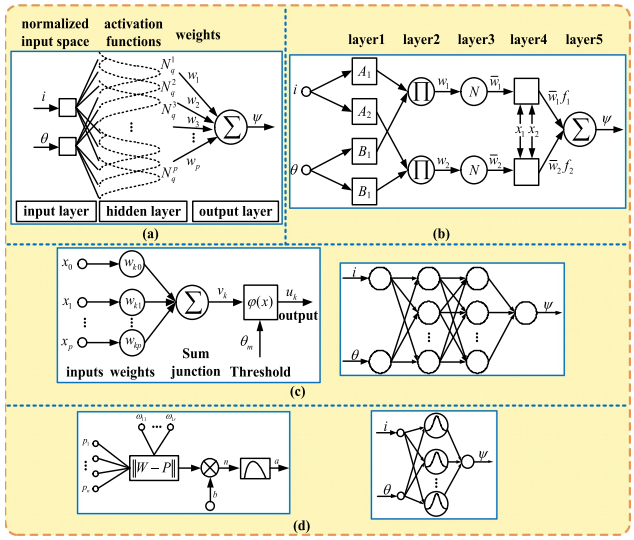

Fig. 33. Architecture of different neural network. (a) Structure of BSNN; (b) A simple multilayer architecture of ANFIS. (c) Structure of a neuron of BPNN and topology of the proposed BPNN. (d) Topology of RBF flux model and structure of a RBF with i inputs.

of DSP, resulting in longer running time and poor high-speed performance. Therefore, a better alternative to the LUT method is urgently needed.

3) Inductance Estimation and Resistance Mismatch: The inductance is of high nonlinearity due to the saturation effects. Generally, the predicted torque is related to the real-time estimated inductance. Thus, the MPC control performance is highly depended on the accuracy of the inductance estimation. To improve the inductance estimation performance, in [22], an additional flux model is generated to ensure the Lyapunov stability of the inductance estimator, and a discrete time adaptive estimation algorithm known as recursive least-squares (RLS) is employed to eliminate the mismatch between actual inductance and static test inductance during operation. In [23], the RLS is used to estimate the inductance and a closed-loop adaptive estimator is developed from the flux model. This estimator needs to be separated from the MPC and Kalman filter loops to ensure stability so that the inductance and resistance can be calibrated online. In real operation, the stator resistance will also change with the rising of temperature, which may also affect the control performance of the MPC. In [24], by selecting the appropriate current tracking error weight factor in the optimal solution of CCS–MPCC, the resistance change does not have a significant impact on the current and torque of the motor, thereby improving the control system's ability to cope with resistance mismatch.

4) Magnetic Characteristic Model: For a concise SRM drive, storing complicated parameter characteristics is not attractive since it occupies large memory and requires more offline effort in parameter measurement. There is an approach to find an analytical expression for each parameter curve instead of store the data in LUTs, which requires a large memory to provide adequate precision.

Once magnetic characteristics are obtained by FEA or through experiments, curve fitting techniques are used to find analytical expressions that properly represent the curves. The approach to model building can be divided into several main categories. Table II shows the comparison of the basic features of some representative parameter modeling methods.

1) *Mathematics model:* An exponential function modeling method was originally proposed in [53] and optimized in [54] and [55]. Curve fitting of fourth-order polynomials [56] and Fourier series extension methods are proposed to estimate parametric curves [57], [58], [59]. In [59], MPTC based on polynomial-Fourier-series model reduces the torque ripple caused by model inaccuracies. In [18], a method for estimating current and torque based on Hermite interpolation with only need for flux characteristics of the aligned and unaligned rotor positions is proposed. Mathematical models can be diverse, but in order to improve modeling accuracy, the model will become more complex.
2) *Neural network (NN) model:* In [60], a 2-D B-spline neural network (BSNN) is designed to model the SRM. In [61], three effective algorithms for modeling of SRM are investigated, which are based on subregional mathematical model, adaptive neural fuzzy inference systems (ANFIS), and NN, respectively. Fig. 33 shows the architecture of them. The inputs are the rotor position and phase current, and the outputs can be the flux-linkage, inductance, and torque. Although NN modeling can achieve high modeling accuracy, the priori data are highly required for training. In addition, the algorithm has poor real-time performance and is difficult to implement online in ordinary control chips.
3) *Other modeling methods:* In [22], the author uses RLS estimator to update each item in the SRM inductor table. At the same time, an interpolation mechanism was introduced and a quantized inductor table was used to improve the accuracy of the reconstruction of the inductor surface. In [62], an unsaturated inductance reconstruction method is proposed to obtain the unsaturated inductance from the saturated incremental inductance under load conditions.

TABLE III
REPRESENTATIVE COST FUNCTIONS

Ref.	Cost function	Objective under consideration	Primary objective	Copper loss	Max current	Excitation states
[63]	$g=\lvert i_{ref}-i_{pre}\rvert$		√	×	×	×
[43,44]	$g=\lvert \psi_{ref}-\psi_{pre}\rvert$					
[25]	$g=\left(T_{ref}-T_{pre}\right)^2$					
[41][64]	$\varepsilon_1=q_1(T_{ref}-T_{pre})^2, \varepsilon_2=q_2\sum_p i_{pre}^2$	$g=\varepsilon_2+\varepsilon_6$	×	√	×	×
[33]	$\varepsilon_3=q_3(\psi_{ref}-\psi_{pre})^2, \varepsilon_4=q_4(s_{k+1}-s_k)$	$g=\varepsilon_1+\varepsilon_2+\varepsilon_4+\varepsilon_7$	√	√	√	√
[32]	$\varepsilon_5=q_5\sum_p \frac{i_p}{i_m}\lvert s_k-s_{k-1}\rvert, \varepsilon_6=q_6(\frac{t_c-t_{d\max}}{T_s}-1-f)^2$	$g=\varepsilon_1+\varepsilon_2+\varepsilon_3+\varepsilon_4$	√	√	×	√
[31]	$\varepsilon_7=I_m=\begin{cases}0 & \text{if } \lvert i_{pre}\rvert\le\lvert i_{\max}\rvert\\ \infty & \text{if } \lvert i_{pre}\rvert>\lvert i_{\max}\rvert\end{cases}$	$g=\varepsilon_1+\varepsilon_2+\varepsilon_7$	√	√	√	×
[18]		$g=\varepsilon_1+\varepsilon_2+\varepsilon_5$	√	√	×	√

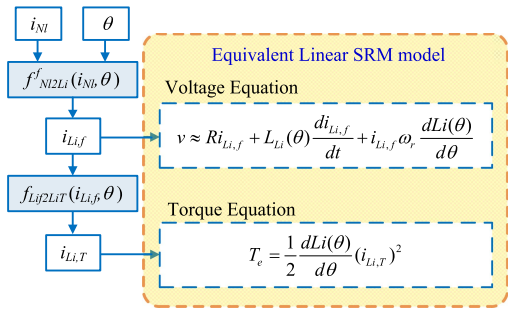

Fig. 34. Process from nonlinear SRM model to equivalent linear SRM model.

5) Equivalent Linear SRM Model: In [31] and [42], the linear-model-based method is proposed. Torque transformation between nonlinear SRM and LSRM is established and the nonlinear SRM model is replaced by the LSRM model. This method is simple and easy to use, but the influence of errors between linear model and nonlinear model in real applications is inevitable.

Fig. 34 shows the process from nonlinear SRM model to equivalent LSRM model, where ω_r is the measured shaft speed, $f^{f}_{Nl2Li}(i_{Nl},\theta)$ is the transformation from nonlinear SRM model to LSRM model with equal flux-linkage, $i_{Li,f}$ is the linear current with equal flux-linkage, $f_{Lif2LiT}(i_{Li,f},\theta)$ is the transformation from linear current with equal flux-linkage to the linear current with equal torque, and $i_{Li,T}$ is the linear current with equal torque. It is noted that the transformation $f_{Lif2LiT}(i_{Li,f},\theta)$ is synthesized from the transformation $f^{f}_{Li2Nl}(i_{Li,f},\theta)$ and $f^{T}_{Nl2Li}(i_{Nl},\theta)$. $f^{f}_{Li2Nl}(i_{Li,f},\theta)$ is the transformation from LSRM model to nonlinear SRM model with equal flux linkage and $f^{T}_{Nl2Li}(i_{Nl},\theta)$ is the transformation from nonlinear SRM model to LSRM model with equal torque.

D. Cost Function

The cost function is the criterion to select the optimal control signal in MPC. Due to different control objects and considered requirements, different MPC use different criteria, namely, cost function. The setting of different objective parameters in the cost function provides diversity to meet different needs [63]. The cost functions used in the literature are summarized in Table III. In the table, ε_2 presents the copper loss, ε_3 presents the flux tracking performance, and ε_4 and ε_5 present excitation states because the excitation states will be determined by the switching states. In ε_6, f is an integer from 1 to N (N is the number of duties to be selected). The larger the duty of the incoming phase is, the smaller the value of f. With $(t_c - t_{d\max})/T_s$, the distance between the present rotor position and the aligned rotor position is measured by T_s. Along with the rotor approaching the aligned position, the duty cycle of the incoming phase will gradually increase. ε_7 is employed to ensure the phase current below the maximum value $i_{\max}$.

For ease of control, the cost function tends to be simple, removing the complex weight selection, considering only the main objective [25], [43], [44], [64]. Some are based on control accuracy and performance, not only considering the primary objective, but also copper loss [18], [31], [32], [33], [41], [65] and flux tracking performance [32]. In addition, for safety reasons, prescribed operating restrictions have been added, such as maximum current [31].

VI. FUTURE TRENDS AND CHALLENGES OF MPC IN SRM

A. Power Converter Topologies

Normally, the AHB converter is the commonly used power converter for SRM drives, which can ensure flexible control and strong fault-tolerant capability. However, the rising cost of power converters cannot be ignored. As shown in Fig. 35, many other power converter topologies, such as full-bridge power converter, three-phase four-leg inverter, C-dump converter, Miller converter, and so on, have also been studied in SRM drive with lower costs.

1) *Full-bridge:* In [66], a control method based on full-bridge power converter is proposed to drive SRM directly, and on this basis, DTC is introduced to suppress the torque ripple. Compared with DTC, MPC has better torque ripple

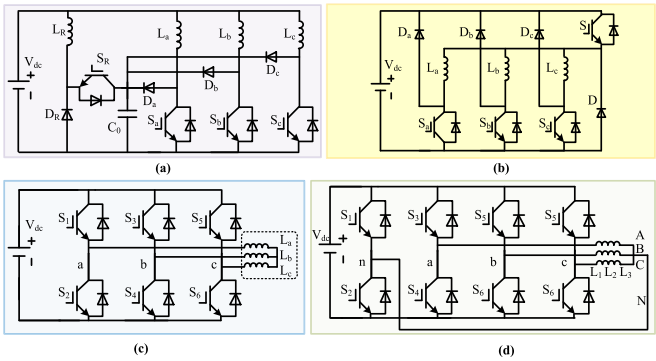

Fig. 35. Other power converter topologies. (a) C-dump converter. (b) Miller converter. (c) full-bridge power converter. (d) three-phase four-leg inverter.

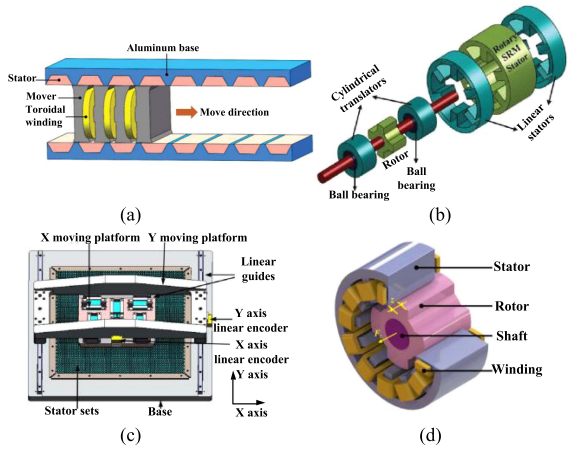

Fig. 36. Structure of these SRMs: (a) LSRM, (b) LRSRM, (c) PSRM, and (d) BSRM.

suppression effect, and the introduction of MPC in full-bridge power converter may get better results.

2) *C-dump converter:* In [67], a resonant C-dump converter controlled by current hysteresis is proposed to solve the voltage resistance problem of the main switching device of conventional capacitor dump converter by using zero-current switching and zero-voltage switching techniques.
3) *Miller converter:* In [68], an improved Miller type SRM converter is proposed to solve the problems of negative torque, high power loss, and low electromechanical conversion efficiency caused by slow demagnetization.

The change of a series of high-performance power converter topology represents an overall improvement in robustness, controllability, and cost and volume reduction for these converters and the implementation of MPC on different SRM power converters seems to become feasible.

It is worth noting that the control mode of SRM varies with different power converters. Therefore, it is necessary to adjust the MPC strategy according to the different converter topology and control characteristics. For example, in the traditional AHB converter, each phase has three operating states, namely "1," "0," and "−1," which, respectively, correspond to positive voltage excitation, zero-voltage continuation, and negative voltage demagnetization, and the control signal is a combination of these three switch states. However, the full-bridge topology is a bipolar control topology that requires a redesign of the switch combination and here "1," "0," and "−1" mean something different. FCS–MPC controls the motor by traversing possible combinations of switching states. Switching state combinations with different definitions result in changes in the FCS–MPC control strategy.

Furthermore, multilevel converters have also been introduced for SRMs because of their potential to enhance high-power and high-voltage machine performance [69], [70]. It also is an alternative to alleviate the low inductance at unaligned rotor position [71]. MPC can solve the complicated control problem caused by multilevel topology. In addition, the advent of a new generation of wide-band gap devices, such as gallium nitride or silicon carbide [72], has greatly increased the control frequency that rate-switching tubes can withstand, which further amplifiers the control effect of FCS–MPC.

B. SRM Topologies

In addition to the control target, the advantages of the control algorithm can also be reflected in different SRM topologies. Design procedures have come up with variations in the structure or operating principle of the machine.

For different motor structures and number of phases, the MPC strategy needs to be adjusted. For example, for FCS–MPC, different phase numbers may cause changes in switching state combinations, and different structures may introduce new control variables and control performance requirements.

Most of the research to date is still based on the conventional SRMs topology, leaving other topologies, such as LSRM, linear-rotary SRM (LRSRM), planar SRM (PSRM), bearingless SRM (BSRM), or disk-type rotor SRM (DTR-SRM) still open for further article. Fig. 36 shows some structure of SRMs.

1) *LSRM:* For the system requiring linear motion, it is less efficient to convert the rotating motion into linear motion by using the rotary motor to drive the crank connecting rod. However, linear motor does not need the crank connecting rod mechanism, and has the advantages of direct drive, small friction loss, adjustable stroke, less noise, higher efficiency, and so on. LSRM has the advantages of both SRM and linear motor. LSRM is mostly used in position control system. In [73], the author proposes robust cooperative positioning control method for the networked composite nested LSRM control systems. Requirements for position accuracy are high when controlling LSRM and it is a good choice to use MPC to improve the accuracy of position tracking.
2) *LRSRM:* LRSRM is generally composed of a rotating stator and a thrust stator. Centralized windings are installed on the rotating stator to provide torque and the thrust stator adopts a wide-toothed structure to provide axial force. Both rotation and linear motion can be realized in LRSRM at the same time which can greatly simplify the structure of the transmission system, effectively reduce the volume and weight, and improve the control accuracy. Most of the researches focus on the study of the motor structure. The relevant control strategies vary with the different

control methods of the motor structure [74]. Unlike conventional rotary motor control, the MPC strategy needs to be adjusted to provide control of torque and axial force.

3) *PSRM:* PSRM is superior in structure, cost, reliability, rapidness, and precision because of eliminating the intermediate mechanical conversion device. However, because there is no buffer of intermediate conversion link, the inherent thrust pulsation and complex nonlinear characteristics of SRM, the precise speed control and position control of switched reluctance planar motor become difficult. In [75], a multistep model position prediction controller for PSRM is proposed in this article, which realizes high precision trajectory tracking motion control of the motor. Thus, using MPC is an effective choice to achieve PSRM high precision position control.
4) *BSRM:* BSRM, which integrates radial magnetic bearing and motor functions, can further improve the power density and its volume and weight are greatly reduced because it does not need independent radial magnetic bearing. BSRM is a multivariable, nonlinear, and strongly coupled complex system. In order to achieve stable suspension and rotation of the motor and improve the performance of the motor, factors, such as core magnetic saturation, two radial suspension forces, and the coupling between torque and radial suspension force, must be considered. To date, predictive control has been implemented on double-windings BSRM [76]. MPC still has great potential to be used in various types of BSRM in the future.
5) *DTR-SRM:* The alignment position of stator and rotor teeth of DTR-SRM has the shortest flux path, and the stator windings are independent of each other, which makes the fault tolerance good. At the same time, it has the characteristics of robustness, controllability, high torque capacity, reliability, and high-power density rating. However, the winding layout of DTR-SRM is different from conventional SRM and will result in a different flux density pattern. Additionally, the rotor pole arcs are substantially greater. When using MPC policy to control DTR-SRM, it needs to be adjusted according to its characteristics.

This is a relatively new research trend, and despite its potential applications, a deep analysis on applying MPC to different SRM topologies has not been investigated.

C. Control Strategies

Although MPC has been successful in some areas of motor drive, it still faces many challenges in the field of SRM drive. FCS–MPC can only select the optimal switch state among the switch states to be selected, and cannot obtain the true optimal switch state. Increasing the number of switch states to be selected improves the control effect but increases the calculation. Therefore, it is not recommended. CCS–MPC can calculate optimal results with complex derivations resulting in a large computational burden. At present, a variety of optimization strategies have been proposed to improve the robustness of MPC and reduce the computational pressure, so that MPC can play the best performance in a wide working range [77]. The above developments in MPC improve its ability to adapt to the complex drives of the future [78].

1) Model-Free and Nested Predictive Control: At present, many scholars in MPC field are trying to improve the modeling accuracy of SRM. Some alternative idea is proposed, such as using model-free predictive control [79] and the elimination of weight factors with nested predictive control [80].

2) Torque Ripple and Vibration Noise Suppression Control: The suppression of torque ripple caused by the inability to track reference values for current or torque remains an urgent issue in the field of the control for SRM. Due to its variable control frequency, FCS–MPC can cause an increase in current ripple. Even though the use of MPC to reduce the source current ripple in the case of bus voltage fluctuations has been proposed in [81], reducing torque ripple caused by current ripple through fixed control frequency is still a necessary research direction. In addition, different combinations of switch states and sector division designs will bring different control effects. These optimization design often leads to a decrease in MPC computation, but at the same time, attention should also be paid to the changes in MPC torque ripple suppression ability.

TSF-based control methods and MPC are all control strategies to suppress the torque ripple. They are combined with each other to achieve better results, which has been introduced above. The TSF-based MPC further suppresses torque ripple and can improve the motor efficiency of SRM. However, it still faces difficulties in selecting the type of TSF and the optimization interval boundaries based on TSF are difficult to accurately set. During the startup and demagnetization stages of the motor, the actual phase torque of SRM is difficult to track the phase reference torque allocated by TSF. Therefore, the bus voltage can be increased by cascading boost converters, thereby further improving the current or torque tracking performance.

To further suppress torque ripple, targeted compensation method can be considered. The simplest compensation strategy is to compensate a fixed value at a fixed position. In order to meet the needs of different operation conditions, real-time dynamic compensation can ensure better results, but it may also lead to an increase in computational power requirements.

The appearance of vibration noise in SRM is mainly caused by the drastic change of radial force in the process of commutation. Normally, the implementation of torque ripple suppression and radial force ripple suppression is often incompatible. To overcome this problem, a series of novel model predictive torque and radial force control strategies are proposed in [82] and [83] to suppress the torque ripple and vibration noise, especially in [83], an online optimal TSF is used to reduce the torque and radial force ripples at a wide speed range. The solutions for eliminating the torque ripple and vibration noise at the same time possess good prospect in SRM drive control system.

3) Sensorless Position Estimation: To ensure high performance operation of the MPC in SRM, the accurate full range position signals is highly required. However, in most industrial applications, the hall sensor based position measurement systems are used, which will result in inaccurate position detection at standstill and low-speed operations. Thus, to apply the MPC in these kinds of SRM systems, the sensorless initial positioning and low-speed real-time position estimation methods are quite necessary. Generally, the high-frequency voltage pulse injection based methods [84] are the key solutions for low-speed

sensorless position estimations. Thus, how to integrate this method with the MPC is still a great challenge needs to be studied.

In the other hand, fast and accurate position sensor is still a difficult problem in hardware manufacturing, and high precision position sensor undoubtedly increases the cost of controller. In order to break through the limitation of position sensing technology, sensorless position estimation methods in medium–high-speed operations are also quite necessary. Generally, for medium–high-speed cases, most of the sensorless position estimation methods are developed based on the flux linkage or inductance characteristics [85], [86]. In most cases, the inductance characteristics are needed to be represented with LUT or other modeling methods in traditional MPC-based SRM control system, which is possible to integrate with those sensorless position estimation schemes for medium–high-speed operations. Thus, it is very desirable to realize the combination of MPC with the full-range sensorless position estimation methods in SRM.

4) Fault-Tolerant Control: In [87], a comprehensive review of the literature on fault diagnosis and control algorithms of SRM drivers is presented, which shows that the SRM possesses very good fault-tolerant capabilities. The torque of SRMs depends on the individual phase contribution and each phase is relatively independent. When a certain phase fails, the control strategy needs to be modified because of the variety of operations and structural differences, which can be simplified by MPC. To date, predictive fault tolerant control has not been applied to SRM drive systems. However, MPC is easier to adjust than other control strategies. The simplest approach is not to adjust any parameters of the MPC because the fault phase is not affected by the control signal. Second, the possible state of the fault phase is not considered, only the state of the normal phase is considered, which reduces the number of switch states required in the calculation of FCS–MPC, and reduces the calculation pressure of the system to a certain extent.

5) High-Speed Control: The features of SRMs determine that the SRMs have outstanding high-speed efficiency and capability to go beyond ultrahigh speed limits. However, due to the computational characteristics of MPC's repeated online optimization, MPC is not suitable for systems with large problem scale or high sampling rate, such as electromechanical systems with fast dynamic changes. Therefore, applying MPC to current SRM driver systems is challenging. With the development of microprocessor performance and the improvement of computing power and computing speed, MPC application in the field of high-speed SRM control is possible.

6) System Robustness Control: Most proposed MPC strategies have considered their ability to handle load disturbances, and experimental verification is provided. MPC can be used to replace traditional PI control. Compared to PI control, MPC avoids the tuning process of control parameters and improves the robustness of the entire system. However, the MPC algorithm, which highly relies on motor parameters, attaches great importance to the problem of mismatches in parameters, such as resistance and inductance during the control process. Although there are currently some measures to deal with the load disturbance and the parameter mismatch, this is still a necessary and worthy direction for further article in MPC.

Usually, the measured or calculated static electromagnetic characteristic data are used as the source for obtaining system parameters during the MPC control process. Traditionally, the LUT methods are used to obtain the flux-linkage and torque from the rotor position and phase current. However, the LUT method consumes a large amount of storage resources and is unable to cope with parameter mismatches during dynamic operation. Therefore, in order to increase the accuracy of parameter acquisition and improve the robustness of the system, NNs are used for SRM modeling [61], [88], [89], [90], [91], [92], [93]. However, the NN-based modeling method sill requires a large amount of prior data and training time. The offline modeling method is based on static electromagnetic characteristic data and cannot take into account the changes in parameters during the dynamic operation of SRM [94], which leading to a decrease in MPC performance. To overcome these problem, many online modeling methods based on BSNN [60], ANFIS [95], and radial basis function NN [96] have been proposed to estimate magnetic flux and torque online by dynamically adjusting algorithm parameters. As compared with the offline modeling schemes, the modeling accuracy and robustness can be highly improved. With the rapid development of artificial intelligence (AI) technology, it is worth looking forward to using more advanced AI algorithms for real-time monitoring and adjustment of SRM parameters.

VII. Conclusion

This article provides a comprehensive overview of the MPC strategies in existing SRM drives, mainly focusing on the following aspects.

1) From the conceptual definition, the basic principles of SRM and MPC are discussed and the development and classification of MPC are explained.
2) From the control object perspective, the main control variables of MPC in the field of SRM control are current, torque, and flux linkage. Based on the above classification, the current article progress has been discussed and corresponding experimental results have been provided to verify the effectiveness of different schemes.
3) From the challenges perspective, the MPC algorithm itself, modeling strategies, cost function construction, and other related issues have been introduced and a detailed analysis of the corresponding solutions have been conducted.
4) The future development trends and challenges of MPC in diversity of power converters, different motor topologies, and the combination of multiple control strategies are discussed in detail which indicates that the newly optimization of MPC strategy in SRM drivers has enormous development potential and will help promote the widespread application of SRM systems in industrial and civilian fields.

References

[1] B. Bilgin, J. W. Jiang, and A. Emadi, *Switched Reluctance Motor Drives: Fundamentals to Applications*. New York, NY, USA: Taylor & Francis, 2018.

[2] D.-H. Lee, J. Liang, Z.-G. Lee, and J.-W. Ahn, "A simple nonlinear logical torque sharing function for low-torque ripple SR drive," *IEEE Trans. Ind. Electron.*, vol. 56, no. 8, pp. 3021–3028, Aug. 2009.

[3] C. Gan, J. Wu, Q. Sun, S. Yang, Y. Hu, and L. Jin, "Low-cost direct instantaneous torque control for switched reluctance motors with bus current detection under soft-chopping mode," *IET Power Electron.*, vol. 9, no. 3, pp. 482–490, 2016.

[4] J. Ye, B. Bilgin, and A. Emadi, "An extended-speed low-ripple torque control of switched reluctance motor drives," *IEEE Trans. Power Electron.*, vol. 30, no. 3, pp. 1457–1470, Mar. 2015.

[5] S. Kouro, P. Cortes, R. Vargas, U. Ammann, and J. Rodriguez, "Model predictive control—A simple and powerful method to control power converters," *IEEE Trans. Ind. Electron.*, vol. 56, no. 6, pp. 1826–1838, Jun. 2009.

[6] J. Rodriguez et al., "State of the art of finite control set model predictive control in power electronics," *IEEE Trans. Ind. Inform.*, vol. 9, no. 2, pp. 1003–1016, May 2013.

[7] L. Guo et al., "An improved model predictive direct torque control method for permanent magnet synchronous generator," *Proc. CSEE*, vol. 36, no. 18, pp. 5053–5061, Sep. 2016.

[8] W. Song et al., "Model predictive flux trajectory tracking control for induction motors operated at low switching frequency," *Proc. CSEE*, vol. 35, no. 12, pp. 3144–3153, Jun. 2015.

[9] D. F. Valencia, R. Tarvirdilu-Asl, C. Garcia, J. Rodriguez, and A. Emadi, "A review of predictive control techniques for switched reluctance machine drives. Part I: Fundamentals and current control," *IEEE Trans. Energy Convers.*, vol. 36, no. 2, pp. 1313–1322, Jun. 2021.

[10] M. Eull and M. Preindl, "A review of virtual-flux model predictive control and receding horizon estimation in motor drives," in *Proc. IEEE Transp. Electrific. Conf. Expo*, Jun. 2021, pp. 439–444.

[11] C. E. Garcia, D. M. Prett, and M. Morari, "Model predictive control: Theory and practice—A survey," *Automatica*, vol. 25, no. 3, pp. 335–348, 1989.

[12] A. Linder, R. Kanchan, R. Kennel, and P. Stolze, *Model-Based Predictive Control of Electric Drives*. Göttingen, Germany: Cuvillier Verlag, 2010.

[13] J. M. Carrasco et al., "Power-electronic systems for the grid integration of renewable energy sources: A survey," *IEEE Trans. Ind. Electron.*, vol. 53, no. 4, pp. 1002–1016, Jun. 2006.

[14] M. Preindl and S. Bolognani, "Comparison of direct and PWM model predictive control for power electronic and drive systems," in *Proc. 28th Annu. IEEE Appl. Power Electron. Conf. Expo.*, Mar. 2013, pp. 2526–2533.

[15] P. Cortes, J. Rodriguez, C. Silva, and A. Flores, "Delay compensation in model predictive current control of a three-phase inverter," *IEEE Trans. Ind. Electron.*, vol. 59, no. 2, pp. 1323–1325, Feb. 2012.

[16] B. Li, X. Ling, Y. Huang, L. Gong, and C. Liu, "An improved model predictive current controller of switched reluctance machines using time-multiplexed current sensor," *Sensors*, vol. 17, 2017, Art. no. 1146.

[17] S. Mehta, P. Pramod, and I. Husain, "Analysis of dynamic current control techniques for switched reluctance motor drives for high performance applications," in *Proc. IEEE Transp. Electrific. Conf. Expo*, 2019, pp. 1–7.

[18] S. Song, R. Hei, R. Ma, and W. Liu, "Model predictive control of switched reluctance starter/generator with torque sharing and compensation," *IEEE Trans. Transp. Electrific.*, vol. 6, no. 4, pp. 1519–1527, Dec. 2020.

[19] A. Anuchin, A. Bogdanov, G. Demidova, E. Stolyarov, D. Surnin, and Y. Vagapov, "Online magnetization surface identification for a switched reluctance motor," in *Proc. 55th Int. Univ. Power Eng. Conf.*, Sep. 2020, pp. 1–5.

[20] H. Oubouaddi, A. Ouannou, L. Kadi, and A. Brouri, "Identification of switched reluctance machine inductance using artificial neuronal network," in *Proc. 2nd Int. Conf. Innov. Res. Appl. Sci., Eng. Technol.*, 2022, pp. 1–6.

[21] F. J. Perez-Cebolla, A. Martinez-Iturbe, B. Martín-Del-Brío, C. Bernal-Ruiz, J. S. Artal-Sevil, and P. Pastor-Flores, "Nonlinear dynamic equivalent circuit of a switched reluctance motor considering core losses and leakage inductance," in *Proc. 45th Annu. Conf. IEEE Ind. Electron. Soc.*, 2019, pp. 1222–1227.

[22] X. Li and P. Shamsi, "Inductance surface learning for model predictive current control of switched reluctance motors," *IEEE Trans. Transp. Electrific.*, vol. 1, no. 3, pp. 287–297, Oct. 2015.

[23] X. Li and P. Shamsi, "Model predictive current control of switched reluctance motors with inductance auto-calibration," *IEEE Trans. Ind. Electron.*, vol. 63, no. 6, pp. 3934–3941, Jun. 2016.

[24] L. Shi, "Predictive current control of switched reluctance motors based on state-space model," M.S. thesis, Hunan Univ., Changsha, China, 2019.

[25] N. Yan, X. Cao, and L. Zhang, "Direct torque control-based model predictive control of switched reluctance motors," *Proc. CSEE*, vol. 37, no. 18, pp. 5446–5453, Sep. 2017.

[26] K. Diao, X. Sun, G. Lei, Y. Guo, and J. Zhu, "Multimode optimization of switched reluctance machines in hybrid electric vehicles," *IEEE Trans. Energy Convers.*, vol. 36, no. 3, pp. 2217–2226, Sep. 2021.

[27] H. Le-Huy and P. Brunelle, "A versatile nonlinear switched reluctance motor model in simulink using realistic and analytical magnetization characteristics," in *Proc. 31st Annu. Conf. IEEE Ind. Electron. Soc.*, 2005, p. 6.

[28] H. Peyrl, G. Papafotiou, and M. Morari, "Model predictive torque control of a switched reluctance motor," in *Proc. IEEE Int. Conf. Ind. Technol.*, 2009, pp. 1–6.

[29] W. Ding, J. Li, and J. Yuan, "An improved model predictive torque control for switched reluctance motors with candidate voltage vectors optimization," *IEEE Trans. Ind. Electron.*, vol. 70, no. 5, pp. 4595–4607, May 2023.

[30] J. Li, W. Ding, J. Yuan, Z. Liu, and R. Hu, "An improved model predictive control method of switched reluctance motor based on direct torque control," in *Proc. 24th Int. Conf. Elect. Mach. Syst.*, 2021, pp. 2568–2572.

[31] G. Fang, J. Ye, D. Xiao, Z. Xia, and A. Emadi, "Computational-efficient model predictive torque control for switched reluctance machines with linear-model-based equivalent transformations," *IEEE Trans. Ind. Electron.*, vol. 69, no. 6, pp. 5465–5477, Jun. 2022.

[32] W. Li, Z. Cui, S. Ding, F. Chen, and Y. Guo, "Model predictive direct torque control of switched reluctance motors for low-speed operation," *IEEE Trans. Energy Convers.*, vol. 37, no. 2, pp. 1406–1415, Jun. 2022.

[33] C. Li, G. Wang, Y. Li, and A. Xu, "An improved finite-state predictive torque control for switched reluctance motor drive," *IET Elect. Power Appl.*, vol. 12, no. 1, pp. 144–151, Nov. 2017.

[34] P. Cortes et al., "Guidelines for weighting factors design in model predictive control of power converters and drives," in *Proc. IEEE Int. Conf. Ind. Technol.*, 2009, pp. 1–7.

[35] R. B. Inderka and R. W. A. A. De Doncker, "DITC—Direct instantaneous torque control of switched reluctance drives," *IEEE Trans. Ind. Appl.*, vol. 39, no. 4, pp. 1046–1051, Jul/Aug. 2003.

[36] W. Ye, Q. Ma, P. Zhang, and Y. Guo, "Torque ripple reduction in switched reluctance motor using a novel torque sharing function," in *Proc. IEEE Int. Conf. Aircr. Utility Syst.*, 2016, pp. 177–182.

[37] X. Xue, K. Cheng, and S. Ho, "A control scheme of torque ripple minimization for SRM drives based on flux linkage controller and torque sharing function," in *Proc. 2nd Int. Conf. Power Electron. Syst. Appl.*, 2006, pp. 79–84.

[38] I. Husain and M. Ehsani, "Torque ripple minimization in switched reluctance motor drives by PWM current control," *IEEE Trans. Power Electron.*, vol. 11, no. 1, pp. 83–88, Jan. 1996.

[39] A. Klein-Hessling, A. Hofmann, and R. W. De Doncker, "Direct instantaneous torque and force control: A novel control approach for switched reluctance machines," in *Proc. IEEE Int. Elect. Mach. Drives Conf.*, 2015, pp. 922–928.

[40] H. Goto and O. Ichinokura, "Model prediction based instantaneous torque control of switched reluctance motor," in *Proc. Int. Conf. Elect. Mach.*, 2014, pp. 810–815.

[41] S. Song, J. Liu, Y. Zhao, L. Ge, R. Ma, and W. Liu, "High-dynamic four-quadrant speed adjustment of switched reluctance machine with torque predictive control," *IEEE Trans. Ind. Electron.*, vol. 69, no. 8, pp. 7733–7743, Aug. 2022.

[42] G. Fang, J. Ye, D. Xiao, Z. Xia, and A. Emadi, "Low-ripple continuous control set model predictive torque control for switched reluctance machines based on equivalent linear SRM model," *IEEE Trans. Ind. Electron.*, vol. 69, no. 12, pp. 12480–12495, Dec. 2022.

[43] A. Xu, C. Shang, J. Chen, J. Zhu, and L. Han, "A new control method based on DTC and MPC to reduce torque ripple in SRM," *IEEE Access*, vol. 7, pp. 68584–68593, 2019.

[44] C. Shang, A. Xu, L. Huang, and J. Chen, "Flux linkage optimization for direct torque control of switched reluctance motor based on model predictive control," *IEEJ Trans. Elect. Electron. Eng.*, vol. 14, no. 7, pp. 1105–1113, Mar. 2019.

[45] D. H. Lee, "Advanced torque control scheme for the high speed switched reluctance motor," in *Advances in Motor Torque Control*. Rijeka, Croatia: InTech, 2011.

[46] H. Liu, Y. Zhao, Y. Fan, and J. Liu, "Torque predictive control based on an improved finite control set model of switched reluctance motor," in *Proc. 7th Int. Conf. Automat., Control Robot. Eng.*, 2022, pp. 126–131.

[47] R. Yuan et al., "A method of torque ripple suppression of SRM based on model predictive control," in *Proc. IEEE Int. Conf. Predictive Control Elect. Drives Power Electron.*, 2021, pp. 229–234.

[48] X. Wen-ping and Y. Jia-wei, "Improved PSO-BPNN algorithm for SRG modeling," in *Proc. IEEE Int. Conf. Ind. Mechatron. Automat.*, 2009, pp. 245–248.

[49] S. Mir, I. Husain, and M. E. Elbuluk, "Switched reluctance motor modeling with on-line parameter identification," *IEEE Trans. Ind. Appl.*, vol. 34, no. 4, pp. 776–783, Jul./Aug. 1998.

[50] J. Corda and S. M. Jamil, "Experimental determination of equivalent circuit parameters of a tubular switched reluctance machine with solid- steel magnetic core," *IEEE Trans. Ind. Electron.*, vol. 57, no. 1, pp. 304–310, Jan. 2010.

[51] L. Ge, J. Zhong, J. Huang, and S. Song, "Model predictive torque control of switched reluctance machine based on torque-balanced measurement and flux-based torque estimation," in *Proc. 24th Int. Conf. Elect. Mach. Syst.*, 2021, pp. 867–872.

[52] S. S. Ahmad and G. Narayanan, "Predictive control based constant current injection scheme for characterization of switched reluctance machine," *IEEE Trans. Ind. Appl.*, vol. 54, no. 4, pp. 3383–3392, Jul./Aug. 2018.

[53] J. V. Byrne and J. B. O'dwer, "Saturable variable reluctance machine simulation using exponential functions," in *Proc. Int. Conf. Stepping Motors Syst.*, 1976, pp. 11–16.

[54] D. A. Torrey and J. H. Lang, "Modeling a nonlinear variable-reluctance motor drive," *Proc. Inst. Elect. Eng.*, vol. 137, pp. 314–326, 1990.

[55] D. A. Torrey, "Switched reluctance generators and their control," *IEEE Trans. Ind. Electron.*, vol. 49, no. 1, pp. 3–14, Feb. 2002.

[56] S. H. Mao and T. C. Tsai, "An analysis of the optimum operating point for a switched reluctance motor," *J. Magnetism Magn. Mater.*, vol. 282, pp. 53–56, Nov. 2004.

[57] X. Li and P. Shamsi, "Adaptive model predictive current control for DSSRM drives," in *Proc. IEEE Transp. Electrific. Conf. Expo.*, Jun. 2014, pp. 1–5.

[58] D. Xiao, S. R. Filho, G. Fang, J. Ye, and A. Emadi, "Position-sensorless control of switched reluctance motor drives: A review," *IEEE Trans. Transp. Electrific.*, vol. 8, no. 1, pp. 1209–1227, Mar. 2022.

[59] L. Ge, J. Zhong, J. Huang, N. Jiao, S. Song, and R. W. De Doncker, "A novel model predictive torque control of SRMs with low measurement effort," *IEEE Trans. Ind. Electron.*, vol. 70, no. 4, pp. 3561–3570, Apr. 2023.

[60] Z. Lin, D. S. Reay, B. W. Williams, and X. He, "Online modeling for switched reluctance motors using b-spline neural networks," *IEEE Trans. Ind. Electron.*, vol. 54, no. 6, pp. 3317–3322, Dec. 2007.

[61] J. Cai, Z. Deng, and Z. Liu, "Nonlinear modeling of switched reluctance motor using different methods," in *Proc. 25th Annu. IEEE Appl. Power Electron. Conf. Expo.*, 2010, pp. 1018–1025.

[62] J. Cai and Z. Liu, "An unsaturated inductance reconstruction based universal sensorless starting control scheme for SRM drives," *IEEE Trans. Ind. Electron.*, vol. 67, no. 11, pp. 9083–9092, Nov. 2020.

[63] V. Yaramasu and B. Wu, *Model Predictive Control of Wind Energy Conversion Systems*. Hoboken, NJ, USA: Wiley, Dec. 2016.

[64] R. Abdel-Fadil and L. Számel, "Enhancement of the switched reluctance motor performance for electric vehicles applications using predictive current control," in *Proc. Int. IEEE Conf. Workshop Óbuda Elect. Power Eng.*, 2018, pp. 195–200.

[65] G. Bhavana, B. L. Narasimharaju, P. Vijaya Vardhan Reddy, and K. Vijay Babu, "Model predictive torque control of switched reluctance motor drive," in *Proc. IEEE 2nd Int. Conf. Elect. Power Energy Syst.*, 2021, pp. 1–5.

[66] N. Yan, X. Cao, and Z. Deng, "Direct torque control of switched reluctance motors based on full-bridge converter," *Proc. CSEE*, vol. 38, pp. 235–242, Aug. 2018.

[67] Y.-H. Yoon, D.-H. Ran, S.-J. Kim, D.-K. Kim, and C.-Y. Won, "Current hysteresis controlled resonant c-dump converter for switched reluctance motor drive," in *Proc. IEEE 35th Annu. Power Electron. Specialists Conf.*, 2004, pp. 1329–1334.

[68] R.-L. Lin, H.-P. Chi, and S.-C. Gu, "High electromechanical efficiency resonant miller-type driver for switched reluctance motors," in *Proc. Int. Conf. Power Electron. Drive Syst.*, 2009, pp. 1211–1215.

[69] F. Peng, J. Ye, and A. Emadi, "An asymmetric three-level neutral point diode clamped converter for switched reluctance motor drives," *IEEE Trans. Power Electron.*, vol. 32, no. 11, pp. 8618–8631, Nov. 2017.

[70] C. Gan, J. Wu, Y. Hu, S. Yang, W. Cao, and J. M. Guerrero, "New integrated multilevel converter for switched reluctance motor drives in plug-in hybrid electric vehicles with flexible energy conversion," *IEEE Trans. Power Electron.*, vol. 32, no. 5, pp. 3754–3766, May 2017.

[71] C. Gan, Q. Sun, J. Wu, W. Kong, C. Shi, and Y. Hu, "MMC-based SRM drives with decentralized battery energy storage system for hybrid electric vehicles," *IEEE Trans. Power Electron.*, vol. 34, no. 3, pp. 2608–2621, Mar. 2019.

[72] A. Bindra, "Wide-bandgap-based power devices: Reshaping the power electronics landscape," *IEEE Power Electron. Mag.*, vol. 2, no. 1, pp. 42–47, Mar. 2015.

[73] L. Qiu, Y. Shi, J. Pan, and B. Zhang, "Robust cooperative positioning control of composite nested linear switched reluctance machines with network-induced time delays," *IEEE Trans. Ind. Electron.*, vol. 65, no. 9, pp. 7447–7457, Sep. 2018.

[74] S. Li, K. W. E. Cheng, N. Cheung, and Y. Zou, "Design and control of a decoupled rotary-linear switched reluctance motor," *IEEE Trans. Energy Convers.*, vol. 33, no. 3, pp. 1363–1371, Sep. 2018.

[75] L. Chen, S.-D. Huang, J.-C. Guo, Z.-Y. Hu, X.-D. Fu, and G.-Z. Cao, "Model predictive position control for a planar switched reluctance motor using parametric regression model," in *Proc. IEEE Int. Symp. Predictive Control Elect. Drives Power Electron.*, 2019, pp. 1–7.

[76] C. Liu, X. Cao, R. Yuan, Z. Deng, and J. Zhou, "Torque sharing and predictive current control of dual-winding bearingless switched reluctance motors for torque ripple reduction," in *Proc. 19th Int. Conf. Elect. Mach. Syst.*, 2016, pp. 1–6.

[77] S. Vazquez, J. Rodriguez, M. Rivera, L. G. Franquelo, and M. Norambuena, "Model predictive control for power converters and drives: Advances and trends," *IEEE Trans. Ind. Electron.*, vol. 64, no. 2, pp. 935–947, Feb. 2017.

[78] A. Salem and M. Narimani, "A review on multiphase drives for automotive traction applications," *IEEE Trans. Transp. Electrific.*, vol. 5, no. 4, pp. 1329–1348, Dec. 2019.

[79] P. G. Carlet, F. Tinazzi, S. Bolognani, and M. Zigliotto, "An effective model-free predictive current control for synchronous reluctance motor drives," *IEEE Trans. Ind. Appl.*, vol. 55, no. 4, pp. 3781–3790, Jul./Aug. 2019.

[80] M. Norambuena, J. Rodriguez, Z. Zhang, F. Wang, C. Garcia, and R. Kennel, "A very simple strategy for high-quality performance of AC machines using model predictive control," *IEEE Trans. Power Electron.*, vol. 34, no. 1, pp. 794–800, Jan. 2019.

[81] L. Ge, J. Zhong, Q. Cheng, Z. Fan, S. Song, and R. W. De Doncker, "Model predictive control of switched reluctance machines for suppressing torque and source current ripples under bus voltage fluctuation," *IEEE Trans. Ind. Electron.*, vol. 70, no. 11, pp. 11013–11021, Nov. 2023.

[82] L. Ge, R. Yuan, Q. Cheng, J. Zhong, C. Bao, and S. Song, "Model predictive torque and force control of an switched reluctance machine," in *Proc. IEEE Int. Conf. Predictive Control Elect. Drives Power Electron.*, 2021, pp. 280–284.

[83] L. Ge, Z. Fan, N. Du, J. Huang, D. Xiao, and S. Song, "Model predictive torque and force control for switched reluctance machines based on online optimal sharing function," *IEEE Trans. Power Electron.*, vol. 38, no. 10, pp. 12359–12364, Oct. 2023.

[84] J. Cai and Z. Deng, "Sensorless control of switched reluctance motors based on full-cycle inductance method," *Trans. China Electrotech. Soc.*, vol. 28, no. 2, pp. 145–154, Feb. 2013.

[85] H. Gao, F. R. Salmasi, and M. Ehsani, "Inductance model-based sensorless control of the switched reluctance motor drive at low speed," *IEEE Trans. Power Electron.*, vol. 19, no. 6, pp. 1568–1573, Nov. 2004.

[86] B. Fahimi, A. Emadi, and R. B. Sepe, "Four-quadrant position sensorless control in SRM drives over the entire speed range," *IEEE Trans. Power Electron.*, vol. 20, no. 1, pp. 154–163, Jan. 2005.

[87] C. Gan, Y. Chen, R. Qu, Z. Yu, W. Kong, and Y. Hu, "An overview of fault-diagnosis and fault-tolerance techniques for switched reluctance machine systems," *IEEE Access*, vol. 7, pp. 174822–174838, 2019.

[88] M. Omar, E. Sayed, M. Abdalmagid, B. Bilgin, M. H. Bakr, and A. Emadi, "Review of machine learning applications to the modeling and design optimization of switched reluctance motors," *IEEE Access*, vol. 10, pp. 130444–130468, 2022.

[89] Y. Cai, Y. Wang, H. Xu, S. Sun, C. Wang, and L. Sun, "Research on rotor position model for switched reluctance motor using neural network," *IEEE/ASME Trans. Mechatron.*, vol. 23, no. 6, pp. 2762–2773, Dec. 2018.

[90] E. Mese and D. A. Torrey, "An approach for sensorless position estimation for switched reluctance motors using artificial neural networks," *IEEE Trans. Power Electron.*, vol. 17, no. 1, pp. 66–75, Jan. 2002.

[91] S. Zhou, "Modeling of switched reluctance motor based on combined clustering RBF network," in *Proc. 20th Int. Conf. Elect. Mach. Syst.*, 2017, pp. 1–5.

[92] W. Ding and D. Liang, "Modeling of a 6/4 switched reluctance motor using adaptive neural fuzzy inference system," *IEEE Trans. Magn.*, vol. 44, no. 7, pp. 1796–1804, Jul. 2008.

[93] D. Liang and W. Ding, "Modelling and predicting of a switched reluctance motor drive using radial basis function network-based adaptive fuzzy system," *IET Elect. Power Appl.*, vol. 3, pp. 218–230, May 2009.
[94] M. Aguado-Rojas, P. Maya-Ortiz, and G. Espinosa-Pérez, "On-line estimation of switched reluctance motor parameters," *Int. J. Adaptive Control Signal Process.*, vol. 32, no. 6, pp. 950–966, Mar. 2018.
[95] X. Yao and Y. Yang, "Online modeling for switched reluctance motors using adaptive network based fuzzy inference system," in *Proc. 29th Chin. Control Decis. Conf.*, 2017, pp. 1568–1573.
[96] Y. Cai, R. Qi, J. Cai, and Z. Deng, "Online modeling for switched reluctance motor using radial basis function neural network and its experimental validation," *Acta Aeronautica et Astronautica Sinica*, vol. 33, no. 4, pp. 705–714, Apr. 2012.

Jun Cai (Senior Member, IEEE) received the Ph.D. degree in electrical engineering from the Nanjing University of Aeronautics and Astronautics, Nanjing, China, in 2012.

From 2013 to 2015, he was a EPSRC Research Associate with the Department of Automatic Control and Systems Engineering, University of Sheffield, Sheffield, U.K. Since 2015, he has been a Professor with the Nanjing University of Information Science and Technology, Nanjing, China. He is also the Academic Dean and a Professor with the School of Mechanical and Electrical Engineering, Anhui Jianzhu University, Hefei, China. His research interests include SR/PMSM drives, EV drive systems, and wireless power transfer.

Prof. Cai is the Fellow of the Royal Society for the Encouragement of Arts, Manufactures and Commerce, and the Senior Member of IEEE and CES.

Xiaolan Dou received the B.Eng. degree in electrical engineering from the School of Automation, Nanjing Institute of Technology, Nanjing, China, in 2021. He is currently working toward the M.Sc. degree in electronic information with the Nanjing University of Information Science and Technology, Nanjing, China.

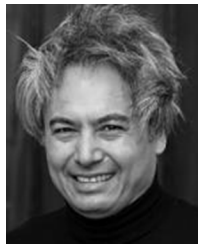

Adrian David Cheok (Senior Member, IEEE) received the Ph.D. degree in electrical engineering from the University of Adelaide, Adelaide, SA, Australia, in 1998.

He is currently a Full Professor with the Nanjing University of Information Science and Technology, Nanjing, China. His research interests include augmented and mixed reality, and power electronics.

Prof. Cheok is the recipient of The Governor General of Australia award. He is IET Fellow.

Wen Ding (Member, IEEE) received the Ph.D. degree in electrical engineering from the Xi'an Jiaotong University, Xi'an, China, in 2009.

He is currently an Associate Professor with the School of Electrical Engineering, Xi'an Jiaotong University. His research interests include electrical machines and drives, and energy conversion systems.

Ying Yan (Member, IEEE) received the Ph.D. degree in electrical engineering from the University of Connecticut, Storrs, CT, USA, in 2018.

He is currently a Lecturer with the School of Automation, Nanjing University of Information Science & Technology, Nanjing, China. His research interests include fault detection and diagnosis.

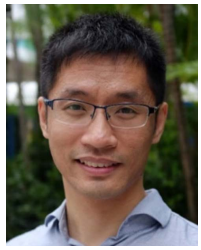

Xin Zhang (Senior Member, IEEE) received the Ph.D. degrees in automatic control and systems engineering from the University of Sheffield, Sheffield, U.K., in 2016, and in electronic and electrical engineering from the Nanjing University of Aeronautics and Astronautics, Nanjing, China, in 2014.

He is currently a Professor with the Zhejiang University, Hangzhou, China. His research interests include power electronics and advanced control theory.